



Methanol synthesis from CO₂ hydrogenation over copper catalysts supported on MgO-modified TiO₂



Chaocheng Liu, Xiaoming Guo*, Qiangsheng Guo, Dongsen Mao*, Jun Yu, Guanzhong Lu

Research Institute of Applied Catalysis, School of Chemical and Environmental Engineering, Shanghai Institute of Technology, Shanghai 201418, People's Republic of China

ARTICLE INFO

Article history:

Received 15 March 2016

Received in revised form

22 September 2016

Accepted 26 September 2016

Available online 28 September 2016

Keywords:

Methanol

CO₂ hydrogenation

MgO-modified TiO₂

Cu surface area

Reducibility

Basicity

ABSTRACT

A serials of copper catalysts supported on TiO₂ modified with different amount of MgO were prepared by an impregnation method and tested for methanol synthesis from CO₂ hydrogenation. The physico-chemical properties of the catalysts were characterized using XRD, N₂ physisorption, N₂O titration, XPS, H₂-TPR and CO₂-TPD techniques. With the increase in amount of MgO, the Cu surface area initially increases and then decreases. The modification of TiO₂ with MgO hinders the interaction between CuO and TiO₂, resulting in a decline in the reducibility of CuO. Furthermore, the number and strength of the moderate and strong basic sites over the surface of catalyst increase with increasing MgO loading. The catalyst exhibits an optimum catalytic activity as the content of MgO is 1 wt%. The CO₂ conversion is determined by the Cu specific surface area and the interaction between CuO and TiO₂, and the CH₃OH selectivity is related to the surface basicity of catalyst.

© 2016 Elsevier B.V. All rights reserved.

1. Introduction

It is believed that the increase in atmospheric CO₂ concentration caused by fossil fuels burning leads to the anthropogenic global warming. Converting CO₂ into valuable chemicals has received much attention as one of the effective CO₂ utilizing technologies. Most researchers focused on the process of CO₂ hydrogenation to methanol because methanol is an important feedstock for the chemical industry and a clean and renewable energy source [1,2].

Methanol synthesis from CO₂ hydrogenation is run mostly on copper catalyst for its inexpensive price and remarkable hydrogenation activity [3,4]. Generally, the amphoteric oxides are chosen as the supporter [5]. Copper catalysts supported on ZnO, Al₂O₃, and ZrO₂ for CO₂ hydrogenation have been investigated intensively in the past few decades [6–14]. TiO₂ is a typical amphoteric oxide, and it possesses the chemical properties similar to that of ZrO₂. However, comparatively few studies on the TiO₂ supported (or promoted) copper catalyst for methanol synthesis have been published. Bando et al. prepared three catalysts (Cu/Al₂O₃, Cu/SiO₂, and Cu/TiO₂) by impregnation method, and they found that TiO₂-supported Cu catalyst showed the highest turnover frequency for

methanol production [15]. Zhang et al. investigated the influences of SiO₂, TiO₂ and TiO₂-SiO₂ promoters on the catalytic performance of CuO-ZnO-Al₂O₃. The results showed that TiO₂ and TiO₂-SiO₂ improved the CuO dispersion and the adsorption of H₂ on catalyst [16]. In a previous work, we disclosed that the introduction of TiO₂ into CuO-ZnO catalyst increased the Cu dispersion and the adsorption capacity of CO₂, and thus improving the catalytic activity and methanol selectivity [17].

According to the dual-site mechanism for CO₂ hydrogenation over the copper catalyst, the adsorption and the activation of CO₂ occur on the surface of supporter [18,19]. Recently, a number of studies showed that the catalytic performance was related closely to the surface basicity of catalyst because CO₂ is intrinsically an acidic molecule [13,14,17]. Therefore, to improve the catalytic performance, several endeavors have been made to tune the basicity of the catalyst [20–22]. In this study, TiO₂ was modified with MgO, one of the most common solid bases, and then copper catalyst supported on the MgO-modified TiO₂ was prepared by an impregnation method. The catalysts were examined by various characterization techniques, and the catalytic activity for methanol synthesis from CO₂ hydrogenation was tested. This study emphasizes the effect of MgO on the physicochemical properties of catalyst. Moreover, the relationship between catalytic behavior and the physicochemical properties was discussed in detail.

* Corresponding authors.

E-mail addresses: guoxiaoming@sit.edu.cn (X. Guo), dsmao@sit.edu.cn (D. Mao).

2. Experimental

2.1. Catalyst preparation

TiO_2 supporter was synthesized by a hydrothermal method. First, 2.0 g hexamethylene tetramine was added to a solvent containing 45.7 mL methanol and 50.0 mL distilled water under stirring, and then 4.3 mL titanium trichloride (15 wt%) was added dropwise into the above solution. The resulting mixture was transferred to a dried Teflon-lined autoclave with a capacity of 200 mL, followed by a hydrothermal treatment at 90 °C for 1 h and 190 °C for 2 h. After the hydrothermal reaction, the white precipitate was collected by centrifuge and washed with ethanol and distilled water until no chloride ion was detected with AgNO_3 solution. Finally, the precipitate was dried in an oven at 80 °C for 12 h and ground into powder.

MgO-modified TiO_2 was prepared by an impregnation method with $\text{Mg}(\text{NO}_3)_2 \cdot 6\text{H}_2\text{O}$ as magnesium source. The amount of MgO, expressed as the ratio of Mg to TiO_2 , ranges from 0.5 to 7 wt%. The impregnated precursor was dried at 110 °C overnight and calcined in air at 400 °C for 4 h.

Copper catalysts supported on TiO_2 and MgO-modified TiO_2 were prepared by an impregnation method with $\text{Cu}(\text{NO}_3)_2 \cdot 3\text{H}_2\text{O}$ as copper source. The nominal Cu loading is 10 wt% of the supporter for all samples. The impregnated samples were dried at 110 °C overnight, followed by a calcination in air at 400 °C for 4 h.

All chemicals used were reagent grade products purchased from Shanghai Chemical Reagent Corporation, Shanghai, China. The synthesized catalysts are denoted as C/x%MT, where C/MT represents copper catalyst supported on the MgO-modified TiO_2 , and x% is the mass ratio of Mg to TiO_2 .

2.2. Catalyst characterization

X-ray diffraction (XRD) analysis of samples was performed on a PANalytical X'Pert diffractometer, applying nickel-filtered $\text{Cu K}\alpha$ radiation with a tube voltage of 40 kV and a tube current of 40 mA. Two theta angles ranged from 20° to 60° with a scanning rate of 5°/min.

The specific surface area was determined with the BET method, using a Micromeritics ASAP2020 M+C adsorption apparatus. The samples were evacuated at 200 °C for 3 h prior to N_2 dosage.

The method of N_2O titration was used to measure the Cu specific surface area (S_{Cu}) over the reduced catalysts [23–25]. Before measurements, catalysts were reduced in situ at 300 °C in a H_2/He flow for 1 h. The samples were flushed in a He flow, and then cooled to the reaction temperature (60 °C). Afterward, a flow of 1 vol% $\text{N}_2\text{O}/\text{He}$ gas mixture was fed into the reactor. A mass spectrometer (Pfeiffer Vacuum Quadstar, 32-bit) was used to detect the amount of the consumption of N_2O . The dispersion of Cu (D_{Cu}) and S_{Cu} were calculated considering a molar stoichiometry of $\text{N}_2\text{O}/\text{Cu} = 0.5$ and a value of 1.46×10^{19} Cu atoms/m² for the copper surface atom density [19]. The Cu average particle size (d_{Cu}) was obtained from the surface area of metallic copper using a spherical particle model [7].

The compositions of catalyst were determined by atomic absorption spectroscopy (AAS) on acid-digested samples, using a SpectraAA-220 Atomic absorption spectrometer (VARIAN).

X-ray photoelectron spectroscopy (XPS) and X-ray-induced Auger electron spectroscopy (AES) measurements were performed on a ESCALAB 250Xi spectrometer using a focused monochromatized Al $K\alpha$ (1486.6 eV). The energy analyzer was set to a constant pass energy of 50 eV. All the binding energy values were calibrated by using C 1s = 284.6 eV as a reference. Quantification of the surface atomic concentrations was carried out using the sensitivity factors supplied by the XPS instrument. In the case of the reduced catalyst, the calcined sample was first transferred to a separate

reaction chamber under ultrahigh vacuum by a transfer rod, and then exposed to a 10% H_2/N_2 flow of 30 mL/min at 300 °C for 1 h. After cooled to room temperature, the reaction chamber was evacuated. The samples were then transferred back to the analysis chamber without exposure to air. For the calcined catalysts, no pretreatment is required before XPS measurement.

Temperature-programmed reduction (TPR) measurements were performed in a linear quartz micro-reactor. Approximately 0.03 g of the catalyst was pretreated with an N_2 at 300 °C for 1 h to remove physically adsorbed water and then cooled down to room temperature. The sample was reduced with a flow of H_2/N_2 gas mixture at a heating rate of 5 °C/min up to 300 °C. The hydrogen consumption for the reduction was monitored by a thermal conductivity detector (TCD).

CO_2 temperature-programmed desorption (CO_2 -TPD) was performed in a self-build apparatus. First, the sample was reduced in a flow of H_2/N_2 gas mixture at 300 °C for 1 h. After cooling down to room temperature, the catalyst was saturated with CO_2 at 50 °C for an hour, and then the physisorbed CO_2 was purged with He flow. TPD of CO_2 was measured by heating the temperature at 5 °C/min, and the desorbed CO_2 was detected by a mass spectrometer. The amount of the desorbed CO_2 was quantitatively calibrated by injecting CO_2 pulses.

2.3. Catalytic testing

The catalytic hydrogenation of CO_2 was carried out using a tubular, flow, high-pressure, fixed-bed reactor. The catalyst sample (0.5 g) was mounted in the reactor and pre-reduced at 300 °C for 3 h in a stream of 10 vol% H_2/N_2 . After cooling to 180 °C, the reactant gas flow ($\text{N}_2:\text{CO}_2:\text{H}_2 = 1:2:6$, molar) was introduced, raising the pressure to 3.0 MPa and the temperature to a given temperature. To avoid any condensation of some products, all post-reactor lines and valves were heated at 140 °C. Effluent products were analyzed by a gas chromatograph (6820, Agilent) equipped with a two-column analytical system, the Porapak Q column and Carbosieve column, which connected to a thermal conductivity detector (CO , CO_2 , N_2) and a flame ionization detector (organic products), respectively. The CO_2 conversion (X_{CO_2}), the CH_3OH selectivity and CH_3OH yield were calculated according to the following equations:

$$X_{\text{CO}_2} = \sum (n * p_i) / [(p_{\text{CO}_2})_{\text{outlet}} + \sum (n * p_i)]$$

$$S_{\text{CH}_3\text{OH}} = p_{\text{CH}_3\text{OH}} / \sum (n * p_i)$$

$$Y_{\text{CH}_3\text{OH}} = X_{\text{CO}_2} * S_{\text{CH}_3\text{OH}}$$

where P_i is the partial pressure of a specific product (labelled as (i)) in the outlet gas, and n stands for the number of carbon atoms in the carbon containing product.

3. Results and discussion

3.1. Textural and structural properties of the catalysts

The XRD spectra of TiO_2 supporter, C/T and C/MT samples were shown in Fig. 1(a). The peaks at 2θ of 25.3°, 37.8°, 48.1°, 54.1° and 55.1° were identified as the diffraction lines of anatase- TiO_2 (JCPDS 21-1272). In comparison with the C/T sample, the diffraction peaks of TiO_2 become weaker and broader with the addition of MgO, suggesting that MgO depresses the crystallization of TiO_2 . The characteristic diffraction peaks of CuO phase appear at 2θ of 35.6° and 38.8° (JCPDS 80-1268). As TiO_2 supporter was modified with a small amount of MgO, no change in the diffraction peak of CuO could be discerned. However, an increase in the diffraction intensity of CuO

Table 1

Physicochemical properties of TiO_2 , C/T and C/MT catalysts.

Sample	$S_{\text{BET}}(\text{m}^2/\text{g})$		$d_{\text{CuO}}^{\text{b}}(\text{nm})$	$d_{\text{Cu}}^{\text{b}}(\text{nm})$	$S_{\text{Cu}}(\text{m}^2/\text{g})$	$D_{\text{Cu}}^{\text{c}}(\%)$	$d_{\text{Cu}}^{\text{c}}(\text{nm})$
	Calcined	Reduced ^a					
TiO_2	121	—	—	—	—	—	—
C/T	80	75	26.4	30.9	1.94	3.51	29.6
C/0.5%MT	91	87	26.1	30.5	2.19	3.93	26.4
C/1%MT	101	97	26.3	30.8	2.31	4.16	25.0
C/3%MT	105	93	28.8	32.3	1.92	3.43	30.3
C/5%MT	100	82	28.7	32.2	1.84	3.24	32.1
C/7%MT	94	83	28.5	32.3	1.75	3.13	33.2

^a After reduction at 300 °C.

^b Calculated with Scherrer equation using the most intense peaks centered at 35.6° and 43.2° for CuO and Cu, respectively.

^c Derived from N_2O titration measurements.

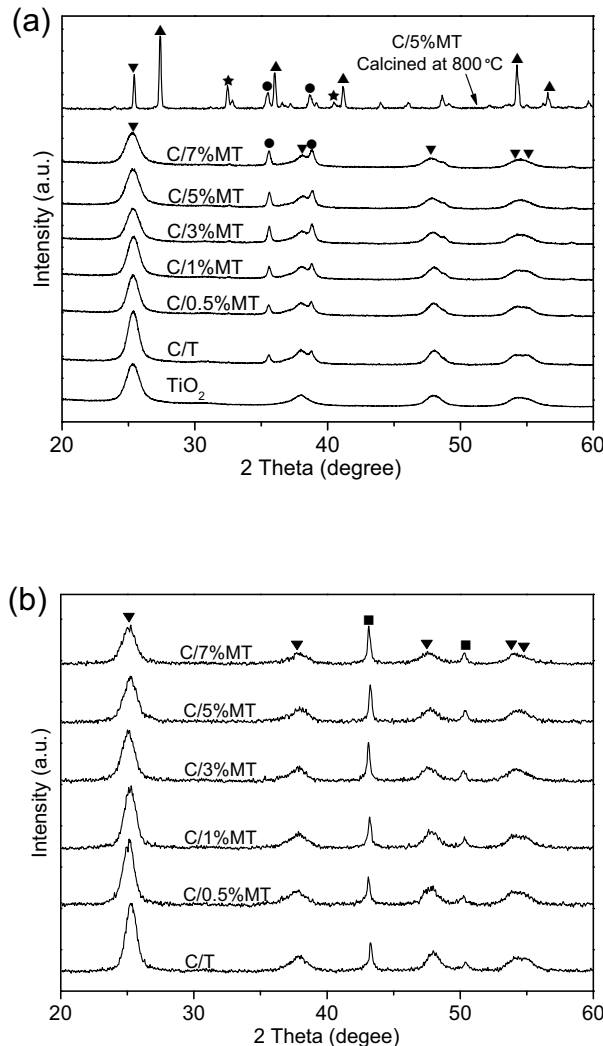


Fig. 1. XRD patterns of TiO_2 , C/T and C/MT catalysts: (a) calcined catalysts, (b) reduced catalysts. TiO_2 (anatase) (\blacktriangledown); TiO_2 (rutile) (\blacktriangle); CuO (\bullet); Cu (\blacksquare); MgTiO_3 (\star).

is observed when the content of MgO reaches 3%. The crystallite sizes of CuO were calculated from the full width at half maximum of diffraction peaks at $2\theta = 35.6^\circ$ with Scherrer equation and listed in Table 1. The CuO crystallite sizes of C/0.5%MT and C/1%MT are close to that of C/T sample. As the content of MgO increases to 3%, the CuO crystallite size increases slightly. Furthermore, as shown in Fig. 1(a), no diffraction peak of MgO can be found for all the studied samples calcined at 400 °C. This is because that the Mg^{2+} ions enter into TiO_2 lattice resulting in the formation of non-crystalline MgTiO_3 .

compound [26–28]. As-formed MgTiO_3 could not be detected by XRD technique due to the low degree of crystallization. To confirm the formation of MgTiO_3 , the sample of C/5%MT was calcined at 800 °C for 4 h and examined by XRD. As shown in Fig. 1(a), after calcining at 800 °C, the characteristic diffraction peaks of MgTiO_3 can be observed at $2q$ of 32.9° and 40.6° (JCPDS 06-0494) [26–28]. Moreover, the diffraction peaks of rutile- TiO_2 appear at $2q$ of 27.4°, 36.1°, 41.3° and 54.4° (JCPDS No. 21-1276), which is attributed to the transformation from anatase- TiO_2 to rutile- TiO_2 as the temperature is higher than 600 °C [26].

The XRD pattern of the catalysts reduced in a flow of H_2/N_2 gas mixture at 300 °C for 1 h is presented in Fig. 1(b). The characteristic diffraction lines at 2θ values of 43.2° and 50.4° correspond to the metallic Cu (JCPDS 01-089-2838). Moreover, for all the samples, the diffraction peaks of CuO disappeared, suggesting that CuO was reduced to Cu completely. The change in the intensity of diffraction lines of Cu from C/T to C/1%MT can not be detected. A further increase of the MgO amount caused a slight rise in the intensity of diffraction lines of Cu. The crystallite sizes of Cu in the reduced catalysts were also calculated with Scherrer equation and listed in Table 1. It can be seen that there is a narrow size distribution (from 30.5 to 32.3 nm) for the crystallite sizes of Cu, in which the differences among them are rather small.

BET surface areas (S_{BET}) of the samples before and after reduction are listed in Table 1. A S_{BET} of 121 m^2/g is obtained over the TiO_2 supporter, and the value of S_{BET} decreases to 80 m^2/g after CuO loading. Comparing with C/T sample, the MgO-modified C/T catalyst exhibits a larger surface area since MgO depresses the crystallization of TiO_2 . After reduction at 300 °C, the BET surface area of catalyst decreases slightly. Copper specific surface area (S_{Cu}) determined by N_2O titration is also shown in Table 1. With the addition of MgO, S_{Cu} increase firstly and then decrease (i.e. a volcano trend), the maximum value is obtained over the sample of 1%CMT. As shown in Table 1, the variation of D_{Cu} with the addition of MgO is similar to that of S_{Cu} , accompanied by an inverse trend of d_{Cu} . This can be explained as follows. On the one hand, the addition of MgO increases the BET surface area, which is favorable for the dispersion of Cu. On the other hand, MgO covers the surface of TiO_2 and weakens the interaction between CuO and TiO_2 , leading to a decrease in the Cu dispersion.

3.2. XPS analysis

The surface chemical state and composition of the catalysts were determined with the XPS technique. The representative photoelectron spectra of the Cu 2p and Ti 2p of the calcined samples are presented in Fig. 2 (a) and (b), respectively. The Cu 2p_{3/2} core line locates at a BE of 933.5 eV together with a shake-up peak centered at 942.9 eV suggesting that the chemical state of copper is Cu^{2+} [13,29]. With the loading of MgO, there is no significant variation in the BE of copper. However, a small shift of the BE of Ti 2p_{3/2}

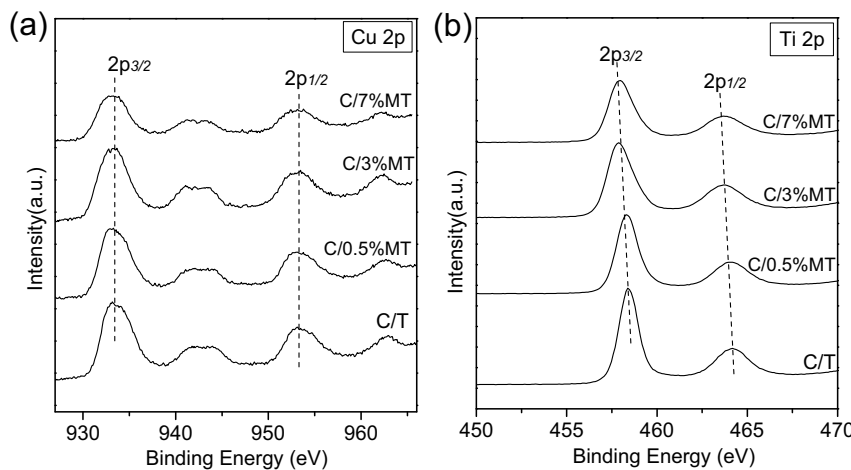


Fig. 2. XPS spectra of the calcined C/T and C/MT catalysts: (a) Cu 2p; (b) Ti 2p.

Table 2
Composition of C/T and C/MT catalysts.

Catalysts	Bulk concentration of metal (at.%) ^a			Surface concentration of metal (at.%) ^b		
	Cu	Mg	Ti	Cu	Mg	Ti
C/T	10.7 (11.2)	–	89.3 (88.8)	15.2	–	84.8
C/0.5%MT	10.7 (11.1)	1.5 (1.4)	87.8 (87.5)	14.2	4.7	81.1
C/1%MT	10.6 (11.0)	2.9 (2.8)	86.5 (86.2)	13.1	9.8	77.1
C/3%MT	10.4 (10.7)	8.2 (8.0)	81.4 (81.3)	11.3	22.2	66.5
C/5%MT	10.3 (10.5)	12.9 (12.6)	76.8 (76.9)	9.1	25.4	65.5
C/7%MT	9.9 (10.2)	17.3 (16.8)	72.8 (73.0)	7.6	29.1	63.3

^a Bulk composition are determined by atomic absorption spectrum; the values in parenthesis are the nominal fraction of metal.

^b Surface composition are determined by XPS.

from 458.4 to 457.9 eV was observed when the content of MgO increases from zero to 7%, which meant that MgO loading changes the electron density of Ti ion. The Mg 1 s core line appears at a BE of 1303.7 eV for all samples, which is indicative of the presence of Mg²⁺ [30]. Surface composition of the calcined catalyst was listed in Table 2. For the C/T sample, the surface concentrations of Cu and Ti are 15.2% and 84.8%, respectively. With the addition of MgO, the surface Cu and Ti concentrations decrease continually, whereas an opposite trend is observed for the surface Mg concentration. As shown in Table 2, compared with the bulk composition, which is very close to the nominal composition for all samples, the surface of catalyst is depleted of Ti. In contrast, a remarkable enrichment of Mg on the surface of catalyst is observed. The occupation of the catalyst surface by Mg hinders the interaction between TiO₂ and CuO leading to a decrease in the dispersion of Cu, which is in accordance with the results of N₂O titration.

The catalysts after in-situ reduction with H₂ were also investigated by XPS. Fig. 3(a) show that the Cu 2p_{3/2} and Cu 2p_{1/2} peaks appear at 931.7 and 951.6 eV, respectively, corresponding to the characteristic of Cu⁰ or Cu⁺ [31]. In addition, the shake-up satellite peak of Cu²⁺ at 942.9 eV disappears, which indicates that there are no Cu²⁺ species left on the surface after reduction [31]. As is well known, XPS cannot differentiate between Cu⁰ and Cu⁺ species because Cu 2p spectra of them are almost identical [31,32]. Cu (LMM) Auger peaks are traditionally used to distinguish Cu⁰ and Cu⁺ since the kinetic energies (KE) of their Auger electrons are separated by approximately 2 eV: Cu⁰ at 918.7 eV and Cu⁺ at 916.8 eV [33]. As shown in Fig. 3(b), for all samples, the KE of Cu (LMM) is about 918.9 eV, demonstrating that Cu⁰ is the predominant copper species on the surface of the reduced catalyst. For element Ti and Mg, XPS spectra of the reduced catalysts are similar to that of the calcined samples under the reduction condition.

Table 3
Temperature of reduction peaks over C/T and C/MT catalysts.

Catalyst	T _α (°C)	T _β (°C)	T _γ (°C)
C/T	146	159	172
C/0.5%MT	147	159	185
C/1%MT	149	159	189
C/3%MT	175	186	216
C/5%MT	183	196	229
C/7%MT	193	202	230

3.3. The reducibility of catalysts

To assess the reduction behavior of the catalysts, TPR measurements were performed. Fig. 4 shows the H₂-TPR profiles of the studied catalysts. All the profiles can be deconvoluted into three Gaussian peaks (dotted curves), and the temperatures of reduction peaks are listed in Table 3. The low temperature peak (α peak) are due to the reduction of CuO surface species; the other two peaks (β and γ peak) appearing in a higher-temperature region correspond to the reduction of bulk-like CuO interacted with TiO₂ strongly and weakly, respectively [29,34,35]. As Fig. 4 shows, when the loading amount of MgO is no more than 1 wt%, apart from a small increase in the temperature of γ peak, there is no significant difference between the MgO-modified and unmodified C/T catalysts. However, as the content of MgO reached 3%, an abrupt increase in the temperature of reduction peak was observed, and the peak maxima of α , β and γ peak appear at 175, 186 and 216 °C, respectively. With a further increase in MgO loading, the reduction peaks shift continually toward the higher temperature.

In general, the reduction behavior of CuO in the catalyst is affected by two factors, the crystallite size of CuO and the interaction between CuO and the supporter. The smaller the crystallite size is, the lower the reduction temperature would be. The results

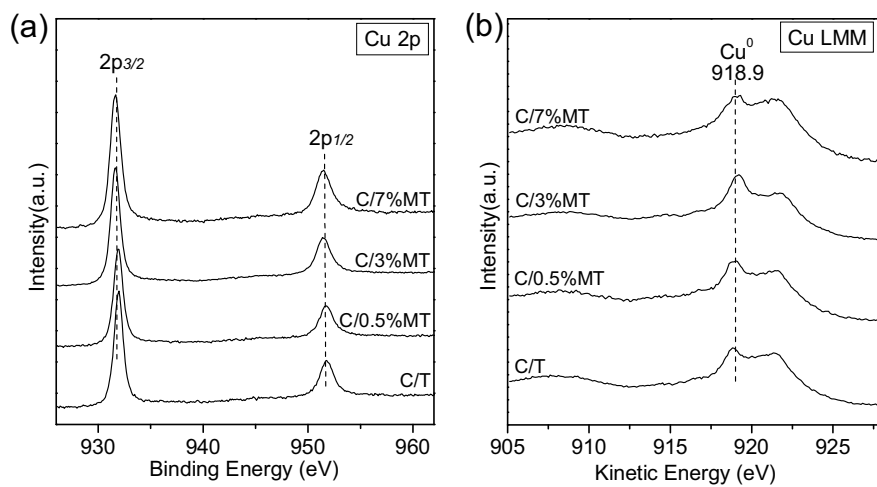


Fig. 3. XPS and AES spectra of the reduced C/T and C/MT catalysts: (a) Cu 2p; (b) Cu LMM.

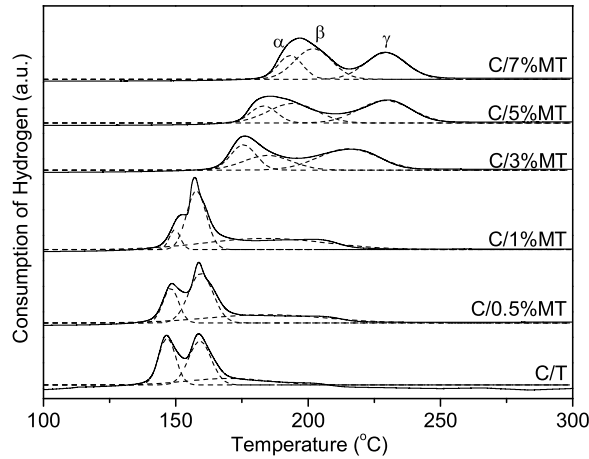


Fig. 4. H₂-TPR patterns of C/T and C/MT catalysts.

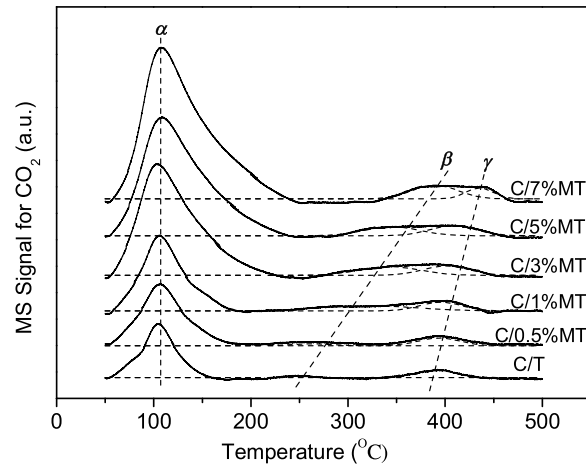


Fig. 5. CO₂-TPD profiles of C/T and C/MT catalysts.

of XRD revealed that the variation of CuO crystallite size was trivial. Therefore, in this study, the shift of the reduction peak of CuO mainly originated from the change in the interaction between CuO and TiO₂. The interaction has a different effect on the reducibility of CuO according to the different supporters. As CuO disperses on the supporter of Al₂O₃ or ZnO, the interaction between CuO and supporter is unfavorable for the reduction of CuO [36,37]; as CuO disperses on ZrO₂ or TiO₂, the interaction results in an easily reducible CuO [37,38]. The interaction probably affects the reducibility of CuO by changing the strength of Cu-O bond [36]. Table 3 show that the temperatures of the reduction peaks over C/T catalyst locate in the range 146–172 °C, well below that of the unsupported CuO (ca. 300 °C) [22,29,36], confirming that the interaction between CuO and TiO₂ facilitates the reduction of the supported CuO. After the modification with MgO, as stated in the part of XPS analysis, the surface of TiO₂ was occupied partly by the component of Mg, especially as the MgO loading reached 3%, which would hinder and weaken the interaction between CuO and TiO₂. The decrease in the interaction leads to a decline in the reducibility of CuO, in other word, an increase in the reduction temperature of CuO. It is noteworthy that the interaction between CuO and supporter related closely to the activity of Cu site formed after reduction [24,29].

3.4. The surface basicity of catalysts

The strength and amount of basic sites on the surface of catalysts were studied by CO₂-TPD. The CO₂ desorption profiles of the prereduced C/T and C/MT are presented in Fig. 5. Additionally, the peak maximum temperature and the number of base sites are listed in Table 4. Three CO₂ desorption peaks (denote as α, β, and γ) can be observed for all the catalysts, and they correspond to weak, moderate and strong base sites according to the strength of base site, respectively. The weak base sites are originated from the surface hydroxyl groups, a Brønsted base. The moderate base sites are associated with the metal-oxygen pairs (i.e. Ti-O pairs in this case), and the strong base sites are related to low coordination oxygen atoms [14,39]. The moderate and strong base sites exhibit typical Lewis basicity. As shown in Fig. 5, after modification by MgO, there is almost no shift in the position of α peak, which means that the change in the strength of weak base site can be neglected. However, a substantial increase in the area of α peak was observed, suggesting a rise in the number of weak base sites. For the peak of β, it shifts toward higher temperature accompanying with an increase in the area. This indicates that MgO modification enhances the strength and number of the moderate base sites simultaneously. A similar variation trend was observed for γ peak with the adding of MgO. It is well known that, as far as oxide is concerned, Lewis basicity is mainly determined by the electronic property of oxygen anion [39,40]. The greater an oxygen anion's electro-donating is,

Table 4

The maximum temperature of CO₂ desorption and the amount of basic site over C/T and C/MT catalysts.

Catalyst	T_α (°C)	T_β (°C)	T_γ (°C)	Number of basic sites ($\mu\text{mol/g}$)		
				Site α	Site β	Site γ
C/T	105	249	390	1.98	0.04	0.32
C/0.5%MT	105	269	392	2.77	0.09	0.37
C/1%MT	105	320	395	3.42	0.57	0.41
C/3%MT	105	339	400	6.66	0.60	0.48
C/5%MT	106	345	408	7.78	0.63	0.52
C/7%MT	107	389	435	9.40	0.70	0.54

the stronger its Lewis basicity will be. The XRD results illustrated that, after the modification with MgO, Ti⁴⁺ in TiO₂ was substituted partly by Mg²⁺. The electronegativity of Mg²⁺ is smaller than that of Ti⁴⁺. Therefore, comparing to the unmodified C/T sample, a higher electro-donating character of oxygen anions neighboring Ti⁴⁺ over the C/MT was obtained, resulting in an increase in the strength of basic sites.

3.5. Catalytic performance

The catalytic properties for methanol synthesis from CO₂ hydrogenation over C/T and C/MT catalysts were presented in Table 5. The main products of the reaction were methanol and CO under the present reaction conditions and traces of methane can be detected at high temperatures.

As Table 5 illustrates, the modification of TiO₂ with a small amount of MgO leads to an increase in the conversion of CO₂. For example, the conversion of CO₂ increases from 4.3% of C/T to 5.2% of C/1%MT. However, a drastic decrease in CO₂ conversion was observed as the MgO loading reached 3%, and the value of CO₂ conversion over this sample is only 3.6%. According to the mechanism of methanol synthesis from CO₂ hydrogenation, the primary role of Cu is to provide a source of atomic hydrogen for the hydrogenation of carbon-containing species by spillover [18,19,41]. Actually, the production of atomic hydrogen includes two steps. First, the molecular H₂ is adsorbed over the Cu active site, and then the adsorbed molecular H₂ dissociates to give atomic hydrogen. The increase in the S_{Cu} only means that more Cu active sites can be provided for the adsorption of H₂ molecules. With regard to the dissociation of the adsorbed H₂ molecule, it relates to the intrinsic activity of Cu site, which is affected by the interaction between Cu and TiO₂. The stronger the interaction, the faster the dissociation rate of H₂ molecule. The results of N₂O titration (Table 1) showed that the modification of TiO₂ supporter by a small amount of MgO gave rise to an increase in the S_{Cu} . Moreover, the results of H₂-TPR indicate that there is no significant change in the interaction between CuO and TiO₂. As a result, more atomic hydrogenation can be produced per unit time for the hydrogenation of carbon-containing intermediates, and a higher CO₂ conversion is obtained over the samples of C/0.5%MT and C/1%MT. When the content of MgO loading increased to 3%, apart from a decrease in the S_{Cu} , H₂-TPR indicated a drastic decline in the interaction between CuO and TiO₂, suggesting that the dissociation of the adsorbed H₂ became more difficult and the rate of producing atomic hydrogen diminished greatly. Therefore, the decrease in both the S_{Cu} and the interaction between CuO and TiO₂ are responsible for the decline in CO₂ conversion as the amount of MgO reaches 3%. To better disclose the relationship between CO₂ conversion and the S_{Cu} , the turnover frequency (TOF) of CO₂ conversion, which represents the molecule number of CO₂ hydrogenated per second per metallic copper atom, was calculated and listed in Table 5. Moreover, a plot of TOF(CO₂) versus S_{Cu} was presented in Fig. 6. The TOF will be a constant if all Cu site in different samples are equally active for the hydrogenation of CO₂ [42,43]. As shown in Fig. 6, the TOF remains almost constant from

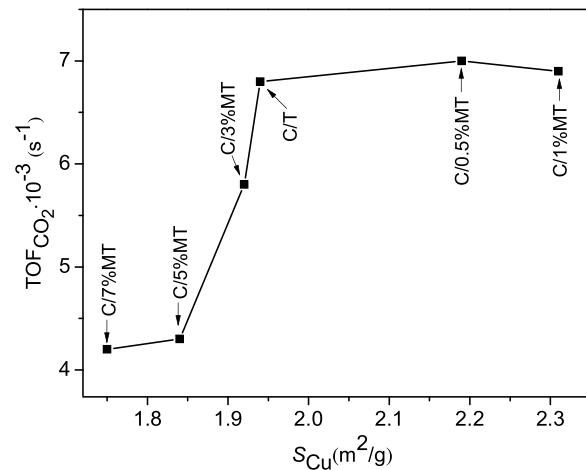


Fig. 6. The relationship between the TOF of CO₂ conversion and the Cu surface area. Reaction conditions: H₂/CO₂ = 3, T = 220 °C, P = 3.0 MPa, GHSV = 4800 h⁻¹.

the sample of CT to C/1%MT corresponding to the S_{Cu} increase from 1.94 to 2.31 m²/g. However, a significant decrease in TOF can be observed for the samples with MgO content from 3 to 7 wt%. The decline in TOF indicates that the activity of Cu site decreases as the amount of MgO reaches 3%, and the reason for this change is ascribed to the decrease in the interaction between CuO and TiO₂. Similar viewpoint was presented in the literature [24,29,43]. Obviously, the results of the TOF (CO₂) confirm further that the CO₂ conversion not only depends on the S_{Cu} but also the interaction between CuO and TiO₂.

As shown in Table 5, the selectivity of methanol increases first and then decreases with increasing the amount of MgO loading. A value of 55.5% was obtained over the C/5%MT catalyst, which increased by 86% compared with the unmodified C/T sample. Although various factors affecting the methanol selectivity have been proposed, no agreement exists in the literature [44–46]. Recently, some researchers disclosed that the selectivity of methanol correlated with the surface basicity of the catalysts [13,14,20–22]. The carbon-containing intermediates adsorbed on the stronger basic site preferred to hydrogenate further to form methanol rather than dissociate to form CO [13,14]. The results of CO₂-TPD show that the strength of moderate and strong basic sites increase continually with the addition of MgO. Consequently, an ascending trend in the CH₃OH selectivity was observed from the unmodified C/T to C/5%MT. As far as C/7%MT is concerned, the decline in CH₃OH selectivity is ascribed to the excessive basicity of the catalyst, which is unfavorable for the activation and hydrogenation of adsorbed intermediates [22]. Similar viewpoint had been proposed by Wang et al. [47].

CH₃OH yield are also listed in Table 5. The CH₃OH yield takes on a volcanic variation trend with the addition of MgO. A maximum value of 1.97% is obtained over the C/1%MT catalyst, and the value increased by 54% in comparison with the unmodified C/T sample. The effects of reaction temperature on the catalytic performance of

Table 5

Catalytic property for hydrogenation of CO₂ to methanol over C/T and C/MT catalysts.

Catalyst	CO ₂ conversion (%)	CH ₃ OH selectivity (%)	CH ₃ OH yield (%)	TOF _{CO₂} × 10 ³ (s ⁻¹)
C/T	4.3	29.8	1.28	6.8
C/0.5%MT	5.0	33.9	1.70	7.0
C/1%MT	5.2	37.9	1.97	6.9
C/3%MT	3.6	48.2	1.74	5.8
C/5%MT	2.6	55.5	1.44	4.3
C/7%MT	2.4	46.0	1.10	4.2

Reaction conditions: H₂/CO₂ = 3, T = 220 °C, P = 3.0 MPa, GHSV = 4800 h⁻¹.

Experimental errors of the CO₂ conversion and CH₃OH selectivity are within ±3% of the values reported.

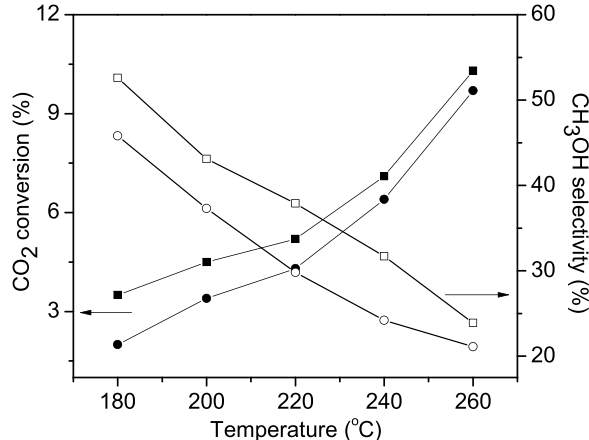


Fig. 7. Effect of temperature on the conversion of CO₂ (solid symbols) and selectivity of methanol (open symbols) over C/T (circles) and C/1%MT (rectangles) catalysts. Reaction conditions: H₂/CO₂ = 3, P = 3.0 MPa, GHSV = 4800 h⁻¹.

C/T and C/1%MT catalysts were studied in the temperature range from 180 to 260 °C, and the results were shown in Fig. 7. With the elevation of reaction temperature, the conversion of CO₂ increases, accompanied by a decrease in CH₃OH selectivity. This trend can be explained in terms of thermodynamics and kinetics, and the related discussion was presented in the literature [12]. Furthermore, it is clear that the CO₂ conversion and CH₃OH selectivity over C/1%MT are higher than those over the unmodified sample of C/T. This proves further that the modification of TiO₂ with an appropriate amount of MgO is favorable for the improvement of the catalytic property of Cu/TiO₂ catalysts.

4. Conclusions

Copper catalysts supported on TiO₂ modified with different content of MgO were prepared and used for the synthesis of methanol from CO₂ hydrogenation. With the addition of MgO, the Cu surface area increases first and then decreases, whereas the interaction between CuO and TiO₂ decreases continually resulting in a decrease in the reducibility of CuO. Moreover, MgO modification increases the strength and number of the moderate and strong basic sites. The CO₂ conversion takes on a volcanic variation trend with increasing the amount of MgO loading, which is a result of the synergistic effect of the S_{Cu} and the interaction between CuO and TiO₂. The CH₃OH selectivity is related to the surface basicity of catalyst, and the appropriate strength of basic sites is beneficial for the CH₃OH selectivity. A maximum methanol yield is obtained at the MgO loading of 1%.

Acknowledgements

The authors thank Shanghai Municipal Education Commission (No. 13YZ117), Shanghai Municipal Science and Technology Com-

mission (No. 13ZR1441200, No.13ZR1461900) and the National Natural Science Foundation of China (No. 21273150) for financial support. The helpful suggestions and linguistic revision of the manuscript provided by the anonymous reviewers are also gratefully acknowledged.

References

- [1] W. Wang, S.P. Wang, X.B. Ma, J.L. Gong, Chem. Soc. Res. 40 (2011) 3703–3727.
- [2] G.A. Olah, A. Goepert, G.K.S. Prakash, J. Org. Chem. 74 (2009) 487–498.
- [3] K.A. Ali, A.Z. Abdullah, A.R. Mohamed, Renew. Sustain. Energy Rev. 44 (2015) 508–518.
- [4] X.M. Liu, G.Q. Lu, Z.F. Yan, J. Beltramini, Ind. Eng. Chem. Res. 42 (2003) 6518–6530.
- [5] T. Tagawa, N. Nomura, M. Shimakage, S. Goto, Res. Chem. Intermed. 21 (1995) 193–202.
- [6] H. Lei, R.F. Nie, G.Q. Wu, Z.Y. Hou, Fuel 154 (2015) 161–166.
- [7] F. Arena, G. Mezzatesta, G. Zafarana, G. Trunfio, F. Frusteri, L. Spadaro, J. Catal. 300 (2013) 141–151.
- [8] R. Raudaskoski, M.V. Niemelä, R.L. Keiski, Top. Catal. 45 (2007) 57–60.
- [9] H.Y. Ban, C.M. Li, K. Asami, K. Fujimoto, Catal. Commun. 54 (2014) 50–54.
- [10] M. Kilo, J. Weigel, A. Wokaun, R.A. Koeppel, A. Stoeckli, A. Baiker, J. Mol. Catal. A: Chem. 126 (1997) 169–184.
- [11] J. Ślęzaki, R. Grabowski, P. Olszewski, A. Kozłowska, J. Stoch, M. Lachowska, J. Skrzypek, Appl. Catal. A: Gen. 310 (2006) 127–137.
- [12] X.M. Guo, D.S. Mao, G.Z. Lu, S. Wang, G.S. Wu, J. Catal. 271 (2010) 178–185.
- [13] X.M. Guo, D.S. Mao, G.Z. Lu, S. Wang, G.S. Wu, J. Mol. Catal. A: Chem. 345 (2011) 60–68.
- [14] P. Gao, F. Li, H.J. Zhan, N. Zhao, F.K. Xiao, W. Wei, L.S. Zhong, H. Wang, Y.H. Sun, J. Catal. 298 (2013) 51–60.
- [15] K.K. Bando, K. Sayama, H. Kusama, K. Okabe, H. Arakawa, Appl. Catal. A: Gen. 165 (1997) 391–409.
- [16] L.X. Zhang, Y.C. Zhang, S.Y. Chen, Appl. Catal. A: Gel. 415–416 (2012) 118–123.
- [17] J. Xiao, D.S. Mao, X.M. Guo, J. Yu, Appl. Surf. Sci. 338 (2015) 146–153.
- [18] I.A. Fisher, A.T. Bell, J. Catal. 172 (1997) 222–237.
- [19] F. Arena, G. Italiano, K. Barbera, S. Bordiga, G. Bonura, L. Spadaro, F. Frusteri, Appl. Catal. A: Gen. 350 (2008) 16–23.
- [20] P. Gao, F. Li, N. Zhao, F.K. Xiao, W. Wei, L.S. Zhong, Y.H. Sun, Appl. Catal. A: Gen. 468 (2013) 442–452.
- [21] P. Gao, F. Li, H.J. Zhan, N. Zhao, F.K. Xiao, W. Wei, L.S. Zhong, Y.H. Sun, Catal. Commun. 50 (2014) 78–82.
- [22] C.L. Zhong, X.M. Guo, D.S. Mao, S. Wang, G.S. Wu, G.Z. Lu, RSC Adv. 5 (2015) 52958–52965.
- [23] G.C. Chinchen, C.M. Hay, H.D. Vandervell, K.C. Waugh, J. Catal. 103 (1987) 79–86.
- [24] J. Ślęzaki, R. Grabowski, A. Kozłowska, P. Olszewski, J. Stoch, J. Skrzypek, M. Lachowska, Appl. Catal. A: Gen. 278 (2004) 11–23.
- [25] O. Hirichsen, T. Genger, M. Muhler, Chem. Eng. Technol. 23 (2000) 956–959.
- [26] R.C. Jin, W.L. Gao, J.X. Chen, H.S. Zeng, F.X. Zhang, Z.G. Liu, N.J. Guan, J. Photochem. Photobiol. A: Chem. 162 (2004) 585–590.
- [27] Z.P. Du, F.S. Chen, Z.K. Lin, X.L. Li, H. Yuan, Y.X. Wu, Chem. Eng. J. 278 (2015) 79–84.
- [28] E.A.V. Ferri, J.C. Sczancoski, L.S. Cavalcante, E.C. Paris, J.W.M. Espinosa, A.T. de Figueiredo, P.S. Pizani, V.R. Mastelaro, J.A. Varela, E. Longo, Mater. Chem. Phys. 117 (2009) 192–198.
- [29] L.C. Wang, Q. Liu, M. Chen, Y.M. Liu, Y. Gao, H.Y. He, K.N. Fan, J. Phys. Chem. C 111 (2007) 16549–16557.
- [30] H.L. Li, X.Y. Wu, J. Wang, Y. Gao, L.Q. Li, K. Shih, Int. J. Hydrogen Energy 41 (2016) 8479–8788.
- [31] L.J. Liu, F. Gao, H.L. Zhao, Y. Li, Appl. Catal. B: Environ. 134–135 (2013) 349–358.
- [32] L.P. Han, L. Zhang, G.F. Zhao, Y.F. Chen, Q.F. Zhang, R.J. Chai, Y. Liu, Y. Lu, ChemCatChem 8 (2016) 1065–1073.
- [33] I. Platzman, R. Brener, H. Haick, R. Tannenbaum, J. Phys. Chem. C 112 (2008) 1101–1108.
- [34] Y.P. Zhang, J.H. Fei, Y.M. Yu, X.M. Zheng, Energy Convers. Manage. 47 (2006) 3360–3367.

- [35] G. Avgouropoulos, T. Ioannides, H. Matralis, *Appl. Catal. B: Environ.* 56 (2005) 87–93.
- [36] F. Arena, K. Barbera, G. Italiano, G. Bonura, L. Spadaro, F. Frusteri, *J. Catal.* 249 (2007) 185–194.
- [37] J. Agrell, H. Birgersson, M. Boutonnet, I. Melián-Cabrera, R.M. Navarro, J.L.G. Fierro, *J. Catal.* 219 (2003) 389–403.
- [38] G.C. Bond, S.N. Namijo, J.S. Wakeman, *J. Mol. Catal.* 64 (1991) 305–319.
- [39] V.K. Díez, C.R. Apesteguía, J.I. Di Cosimo, *Catal. Today* 63 (2000) 53–62.
- [40] M. Verzuiu, B. Cojocaru, J.C. Hu, R. Richards, C. Cioculescu, P. Filip, V.I. Parvulescu, *Green Chem.* 10 (2008) 373–381.
- [41] I.A. Fisher, H.C. Woo, A.T. Bell, *Catal. Lett.* 44 (1997) 11–17.
- [42] M. Boudart, *Chem. Rev.* 95 (1995) 661–666.
- [43] Q. Sun, Y.L. Zhang, H.Y. Chen, J.F. Deng, D. Wu, S.Y. Chen, *J. Catal.* 167 (1997) 92–105.
- [44] S. Fujita, S. Moribe, Y. Kanamori, M. Kakudate, N. Takezawa, *Appl. Catal. A: Gen.* 207 (2001) 121–128.
- [45] J. Toyir, P. Ramírez de la Piscina, J.L.G. Fierro, N. Homs, *Appl. Catal. B: Environ.* 34 (2001) 255–266.
- [46] M.D. Rhodes, A.T. Bell, *J. Catal.* 233 (2005) 198–209.
- [47] G.N. Wang, L.M. Chen, Y.Y. Guo, M.L. Fu, J.L. Wu, B.C. Huang, D.Q. Ye, *Acta Phys. –Chim. Sin.* 30 (2014) 923–931.